Gas-phase Photoluminescence and Photodissociation of Silver-capped Hexagold Clusters

Jean-François Greisch[1*†], Ana Ballester-Caudet[2], Sebastian Volker Kruppa[3], Zhen Lei[4], Quan-Ming Wang[4], Christoph Riehn[3], Françoise Remacle[2]

[1] Institute of Nanotechnology, Karlsruhe Institute of Technology, Hermann-von-Helmholtz-Platz 1 76344 Eggenstein-Leopoldshafen, Germany

[2] Theoretical Physical Chemistry, UR MolSys, B6c, University of Liège, B4000 Liège, Belgium

[3] TU Kaiserslautern, Department of Chemistry and Research Center OPTIMAS, Erwin-Schrödinger-Str. 52–54, 67663 Kaiserslautern, Germany

[4] Department of Chemistry, Tsinghua University, Beijing, 100084, P. R. China

Supporting Information Placeholder

ABSTRACT: We report on the radiative and non-radiative deactivation pathways of selected charge states of the stoichiometric hexagold phosphine-stabilized ionic clusters, $[(C)(AuDppy)_6Ag_2 \cdot (BF_4)_x]^{(4-x)+}$ with x=2 and 3 ($Dppy$ = diphenylphosphino-2-pyridine), combining gas-phase photoluminescence and photodissociation with quantum chemical computations. These clusters possess an identical isostructural core made of a hyper-coordinated carbon at their center octahedrally surrounded by six gold ions, and two silver ions at their apexes. Their luminescence and fragmentation behavior upon photoexcitation was investigated under mass and charge control in an ion trap. The experimental and computational results shed light on the electronic states involved in the optical transitions as well as on their core, ligand, or charge transfer character. Gas-phase results are discussed in relation with condensed phase measurements, as well as previous observations in solution and on metal-organic frameworks. The monocationic species (x=3) is found to be less stable than the dicationic one (x=2). In the luminescence spectrum of the monocationic species a shoulder at short wavelength can be observed and is assigned to fragment emission. This fragment formation appears to be favored for the monocation by the existence of a low lying singlet state energetically overlapping with the triplet state manifold, which is populated quickly after photoexcitation.

INTRODUCTION

Ligated polynuclear gold clusters with an intense and long-lived room temperature luminescence in the visible spectral range as well as the ability to form nanoscale architectures are promising OLED emitters, photochemical converters, and luminescent reporters for sensing or imaging.[1-16] The photophysical properties of such clusters have been found to be highly sensitive to the nuclearity, the size and shape of the cluster core, the nature of the coordinating ligands, as well as the Au-Au distances.[17-21] The impact of counterions, on the other hand, has been neglected so far. Furthermore, since metal-organic frameworks (MOFs) assembled from luminescent clusters have been found to display a marked dependence of their luminescence on the solvent molecules filling their channels,[8] a deeper understanding of the interactions between the subunits as well as a description of the nature of the emission is needed.

In gold nanocrystals slightly larger than the metal's Fermi wavelength (~0.5 nm for Au), energy levels are quantized with profound consequences on optical, electronic, charging, and transport processes even under ambient conditions.[22-23] Not only does catalytic and electrocatalytic activity emerge but also enhanced optical properties such as strong nonlinear or electro-optical effects. For the even smaller clusters investigated here (~0.4 nm Au core), distinctive quantum confinement effects occur. In particular, broad collective resonances completely give way to discrete electronic transitions among quantized levels resulting in a discrete electronic structure and molecule-like properties such as intrinsic magnetism and enhanced photoluminescence.[4, 23-25]

Overall, the properties of gold clusters, formally formed here of Au(I) atoms (closed-shell $5d^{10}$ electronic configuration), are governed by 1) relativistic effects involving high-speed core electrons moving close to the Au nuclei; this causes an increase in the effective nuclear charge leading to a radial contraction and stabilization of the less-diffuse orbitals (such as the 6s and 6p orbitals), while more-diffuse orbitals (such as the 5d-orbitals) expand due to the enhanced shielding effect by the contracted s/p-orbitals;[18, 20] 2) configuration mixing of the 5d-orbitals with hybrid orbitals of appropriate symmetry derived from the 6s and 6p orbitals, reportedly responsible for Au(I) ⋯ Au(I) stabilizing interaction and Au(I) – C bonding interaction,[17-21] and 3) electron correlation.[17-18, 26] Altogether, these three effects are often designated by the term "aurophilic" interactions. Due to a very strong spin−orbit coupling, excited singlet state populations of gold clusters also typically undergo a fast intersystem crossing[27] to the triplet manifold followed by long-lived luminescence. Additionally, some optical transitions are sensitive to the surrounding environment as a consequence of their charge transfer character or formation of solvent exciplexes,[28-29] corresponding either to a ligand-to-metal charge transfer (LMCT) or a metal-to-ligand charge transfer (MLCT).[30]

Unlike ligand-protected Au clusters with core structure and surface motif,[4-5, 31] the carbon hypercoordinated cluster studied here,

$[(C)(AuDppy)_6Ag_2 \cdot (BF_4)_4]$ abbreviated $[\mathbf{1} \cdot (BF_4)_4]$, contains an octahedral Au_6 core with two Ag atoms capping two opposite Au_3 triangles, and six peripheral $Dppy$ ligands.[32-33] The hexagold core with its interstitial carbon is characterized by short Au–Au contacts along the edges of the polyhedra.[32] Its structure is similar to that of the hexaauriomethane $[(C)(AuPPh_3)_6] \cdot (CH_3OBF_3)_2$ (PPh_3 = triphenylphosphine) cluster first reported by Schmidbaur and coworkers.[34] When considering the coordination of the silver atoms by diphenylphosphino-2-pyridine ligands, the $[\mathbf{1}](BF_4)_4$ cluster can be described as the fusion of two $AgAu_3$ tetrahedral moieties sharing a carbon center, each moiety similar to $[(E)(AuDppy)_3Ag \cdot (BF_4)_2]$ with $E = O$, S, or Se heterometallic clusters.[1] The heterometallophilic Au–Ag interaction contributes, concurrently with the diphenylphosphino-2-pyridine ligands, to their stabilization. This affects the charge transfer dynamics as well as the photophysical and spectroscopic properties of the $[\mathbf{1} \cdot (BF_4)_4]$ cluster which is characterized by i) an energy gap small enough that absorption in the visible region occurs, ii) ultrafast intersystem crossing (1−3 ps), iii) solvent dependent energy transfer, and iv) temperature dependent intensity of the phosphorescence in solution. [28, 32] The cluster room-temperature quantum yield of luminescence in solution (ϕ =0.29)[32] is comparable to that of another set of systems stabilized by heterometallophilic Au···M bonding, the heterometallic copper-gold alkynyl complexes reported by Koshevoy *et al.* (ϕ =0.9).[35]

In dichloromethane at room temperature, the $[\mathbf{1} \cdot (BF_4)_4]$ cluster is characterized by an absorption onset about 475 nm, a red emission with maximum between 600 and 640 nm (λ_{ex} = 350nm), and a single-exponential luminescence decay behavior with a luminescence lifetime of 5.7 µs.[28, 32] Analysis by Zhou *et al.* of femtosecond time-resolved transient absorption experiments in solution using a sequential model yields excited state dynamics by three different states (1) ^{1}MLCT(Au) state (τ = 1−3 ps); (2) ^{3}MLCT(Au) state (τ = 11−40 ps), and (3) ^{3}MLCT(Ag) state (long-lived) whose relative population can be modulated by the solvent's polarity and hydrogen bonding ability.[28] The triplet nature of the solution emission is supported by the significant redshift of the emission compared to the absorption, the long luminescence decay, as well as excited-state absorptions and dynamics obtained from the femtosecond time-resolved transient absorption experiments. In absence of information about the counterions, the emission of the $[\mathbf{1}](BF_4)_4$ cluster also appears remarkably insensitive to the nature of the solvent[28] while porous metal–organic frameworks formed upon silver binding of the $[(C)(AuMdppz)_6](BF_4)_2$ ($Mdppz$ = 2-(3-methylpyrazinyl)-diphenylphosphine) derivative display significant solvatochromism as well as a possible dual emission.[8]

In this work, mass spectrometric selection enables the separate investigation of stoichiometrically homogeneous ensembles of clusters characterized by different numbers of tetrafluoroborate counterions.[31] The photoluminescence and photodissociation of the mass-selected $[\mathbf{1} \cdot (BF_4)_x]^{(4-x)+}$ with $x = 2,3$ clusters *in vacuo* yields complementary information about their radiative and non-radiative electronic deactivation pathways. Furthermore, given that the investigated species are stored in the gas phase in an ion trap, their structure, electronic, and optical properties are unconstrained by solvent or environmental effects (packing or more generally coupling to the environment). The experimental results can thereby be directly compared to computations, providing benchmarks for computational approaches. On the application side, the present study offers a first insight into the impact of counterions and possible dynamical equilibria on the luminescence properties of gold cluster salts.

EXPERIMENTAL AND COMPUTATIONAL

Materials

The synthesis of $[\mathbf{1}](BF_4)_4$ by Wang and co-workers was reported elsewhere.[32] The purified solid sample was stored in the dark until dissolution in dichloromethane or acetonitrile for electrospray ionization. The composition of the electrosprayed species has been unambiguously established using a SYNAPT G2S-HDMS mass spectrometer (Waters, Manchester).

Gas-phase photoluminescence

The gas-phase luminescence spectra were acquired using the setup previously described in Ref. 36 and subsequently modified to measure the gas-phase photoluminescence of lanthanoid cluster-like complexes.[37-38] Briefly, it consists of a homebuilt temperature-regulated (down to 82 K) quadrupole ion trap. After being nano-electrosprayed from a ~10^{-4} M dichloromethane (LC-MS grade) solution using borosilicate capillaries, the ions are mass-selected and trapped before being photoexcited either using a Toptica iBEAM-SMART-405-S (405 nm) or using a Ar^+-laser (Spectra Physics 2080-15S) (458 nm and 476 nm lines), while being thermalized by collisions with a helium buffer gas at a pressure of ~0.2 mbar in order to prevent photo-induced fragmentation. Ion photoluminescence is collected perpendicularly to the excitation beam by a Zeiss EC PlanNeofluor 5x/0.15 microscope objective imaging the ion cloud *via* a 3mm diameter aperture in one of the endcaps. It is then filtered to eliminate scattered excitation light using long pass filters before being focused into a fiber and sent to a spectrograph (SpectraPro 300i, Acton Research, Roper Scientific) equipped with 150 grooves/mm gratings and an electron-multiplying charge coupled device for detection (Idus DV-401A-BV, Andor).

Time resolved measurements are performed using a diode laser (405 nm, Toptica iBEAM-SMART-405-S) operated in pulsed mode (500 ps rise and 800 ps fall times). Instead of into a fiber, the collected ion luminescence is focused directly onto the aperture of a photomultiplier (Hamamatsu H7421-40) coupled to a multiple-event time digitizer (P7888, FAST ComTec).

Gas-phase photodissociation

UV-Vis electronic action spectra of mass-selected ions were obtained employing photodissociation (PD) spectroscopy as described elsewhere.[39-42] Briefly, a ~10^{-4} M acetonitrile (LC-MS grade) solution of $[\mathbf{1}](BF_4)_4$ was electrosprayed in positive mode (Apollo II electrospray source, Bruker Daltonics) at an infusion rate of 100 µl/h assisted by nitrogen sheath gas (ca 6 psi, 414 mbar). The ions of interest (integer nominal masses m/z 1580, 1536, 1024, 995, see Table 1) were isolated selecting their full isotope pattern, fragmented by laser irradiation, and subsequently mass analyzed in a customized 3D quadrupole ion trap mass spectrometer (amaZon speed, Bruker Daltonics). Hereby, a shutter was synchronized with the mass spectrometer in order to irradiate the ions only in a 100 ms storage time window (~98 laser pulses per stored ion ensemble). The abundance of species m/z 1536 and 995 was enhanced by collisional-induced dissociation (CID) of isolated m/z 1580 and 1024 precursor species and isolated for subsequent photodissociation (MS^3 step). The femtosecond laser system used is based on a Ti:sapphire chirped pulse cryogenic regenerative amplifier (Wyvern 1000^{TM}, KMLabs) whose output pulse train (~ 780 nm, FWHM ~ 30nm, ~ 4W, 982 Hz, Δτ ~ 50 fs) was used to pump two identical nonlinear frequency converters (TOPAS-C, Light Conversion, abbrev. TC_1 and TC_2). The resulting beams (TC_1: 283-403 nm, TC_2: 400-480 nm) were attenuated to 2 µJ/pulse using a neutral density filter, focused onto the ion trap center (~ 1 mm diameter) and spatially overlapped with the ion cloud. Either of the beams (TC_1, TC_2) were used to obtain photodissociation action spectra. These were acquired stepwise (3-5 nm steps) by averaging at least 160 individual mass spectra

for each wavelength position. From the resulting mass spectra the total fragment yield (*TFY*) was calculated as $TFY = \frac{\sum_i F_i}{\sum_i F_i + P}$ and normalized to the number of photons $N = E_{pulse} \cdot \frac{\lambda}{h \cdot c}$, where $\sum_i F_i$ is the sum of all fragment ion signals and P represents the integrated mass peak intensity of the precursor species. Color changes in Figure 3 indicate a change in the nonlinear output scheme or wavelength filters requiring a re-optimization of the laser beam / ion cloud overlap. The respective spectral regions were scaled by factors determined from overlapping wavelength points.

Quantum Chemical Calculation

The computed gas-phase equilibrium geometries of the $[\mathbf{1} \cdot (BF_4)_x]^{(4-x)+}$ ions, with $x = 1,2,3$, are based on the crystal structure reported by Wang et al.[32] The electronic structure computations were carried out at the density functional theory level as implemented in the Gaussian 09[43] quantum chemistry suite of programs. The long-range corrected functional CAM-B3LYP[44] was used. It is well suited on the one hand to account for the description of the electrostatic and non-covalent interactions between the metallic core and the tetrafluoroborates, as well as the non-covalent interactions between the ligands, and on the other hand, to describe excited states with moderate charge transfer.[45] Relativistic effects were included using relativistic energy corrected pseudo-potentials and double-zeta basis set LANL2DZ[46-47] for the gold and silver atoms. The 6-31G(d,p) Gaussian basis set was used for the other atoms. Equilibrium geometries of the ground and excited states were determined. Both singlet and triplet excited states were computed with the linear response TD-DFT methodology and the absorption and emission spectra obtained by convolution of the obtained stick spectra with Gaussian line shapes (as detailed in the captions). Partial charges on nuclei were computed using the natural population analysis (NPA) and the natural bond orbital (NBO) methodology.[48-49]

RESULTS AND DISCUSSION

Mass spectrometry and ground state computational results

Upon nanospraying $[\mathbf{1}](BF_4)_4$ solubilized in dichloromethane, one primarily observes the $[\mathbf{1} \cdot (BF_4)_3]^+$ and $[\mathbf{1} \cdot (BF_4)_2]^{2+}$ species (see Figure S1). Under mildly activating source conditions or when spraying from more polar solvents such as acetonitrile, the $[\mathbf{1} \cdot (BF_4)_3]^+$ species vanishes and the $[\mathbf{1} \cdot (BF_4)_2]^{2+}$ species, which retains only two tetrafluoroborates, dominates as shown in Figure 1.

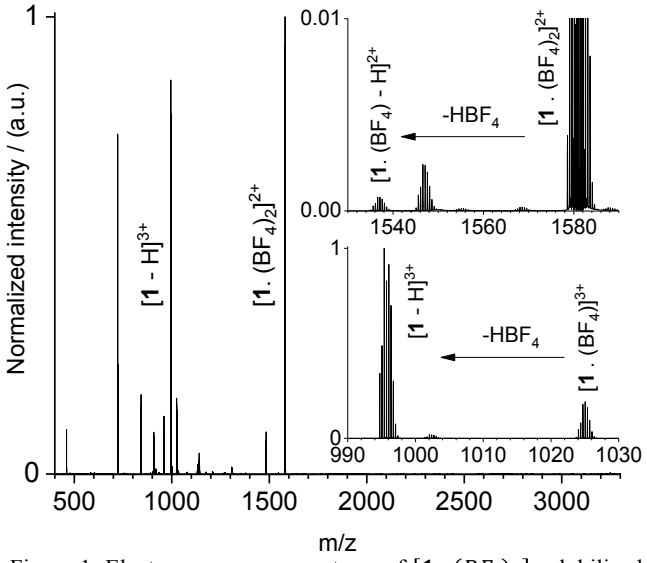

Figure 1. Electrospray mass spectrum of $[\mathbf{1} \cdot (BF_4)_4]$ solubilized in dichloromethane. The species formed under mildly activating in-source conditions upon HBF4 loss are shown in the inset.

Besides the $[\mathbf{1} \cdot (BF_4)_2]^{2+}$ dication, one also observes, as minority species in Figure 1, the doubly charged $[\mathbf{1} \cdot (BF_4) - H]^{2+}$ cluster at *m/z* 1537.06 (most abundant isotopologue) formed by loss of HBF_4 from the precursor. The second most intense species under these conditions is the triply charged $[\mathbf{1} - H]^{3+}$ at *m/z* 995.70 likely a product of the marginally abundant $[\mathbf{1} \cdot (BF_4)]^{3+}$ species (*m/z* 1025.04) upon HBF_4 loss. Consequently, from the very low abundance of the mono-charged cluster ion sprayed from acetonitrile or from dichloromethane under mildly activating conditions and the composition of the observed species, it is suggested that a maximum of two tetrafluoroborates bind strongly enough to the cluster to be easily observed in the gas-phase.

This is further supported by the results of computations that predict the existence of two binding sites with different computed binding energies for the tetrafluoroborate (Figure 2-a,b). Sites A and B are characterized by a tetrafluoroborate binding energy of -766 kJ/mol and -722 kJ/mol, respectively, and a distance from the boron atom to the central carbon of 4.396 Å and 7.519 Å, respectively. It appears therefore that the first pair of tetrafluoroborates, leading to the formation of the $[\mathbf{1} \cdot (BF_4)_2]^{2+}$ species, is preferentially located belt-wise (close to the gold) while the second pair, leading finally to the formation of the neutral $[\mathbf{1} \cdot (BF_4)_4]$ species, is in the vicinity of the silver atoms. Isomers of the $[\mathbf{1} \cdot (BF_4)_x]^{(4-x)+}$ ions with $x = 2,3$ investigated at the PM7 level prior reoptimization at the CAM-B3LYP level are displayed in Figure S2.

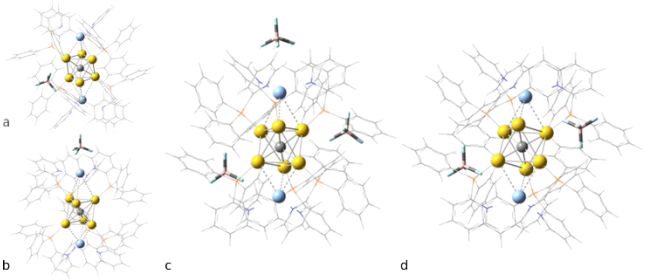

Figure 2. Equilibrium geometries of the ground state of the $[\mathbf{1} \cdot (BF_4)_x]^{(4-x)+}$ species with x=1,2, and 3. (a-b) $[\mathbf{1} \cdot (BF_4)]^{3+}$ two binding sites for the tetrafluoroborate: site A (a) close to the gold atoms and site B (b) closer to the silver atom. (c-d) the computed equilibrium geometries of $[\mathbf{1} \cdot (BF_4)_3]^+$ (c) and $[\mathbf{1} \cdot$

$(BF_4)_2]^{2+}$ (d) at the CAM-B3LYP level. Tetrafluoroborates are represented as capped sticks while Au atoms, Ag atoms and the central carbon atom are represented as yellow, pale blue and grey spheres, respectively. The diphenylphosphino-2-pyridine ligand shell ($Dppy$) is composed of P atoms (orange), phenyl rings with C (grey), pyridine ring (N in blue) and H atoms (white) in wireframe representation.

The mass spectrometric observation (Figure 1) of the species $\left[\mathbf{1}-H\right]^{3+}$ and $\left[\mathbf{1}\cdot(BF_4)-H\right]^{2+}$ – both resulting from a HBF_4 loss – and the absence of signal corresponding to the quadruply charged $[\mathbf{1}]^{4+}$ cluster indicates that upon gas-phase dissociation, as expected, the release of the counterion as a negatively charged tetrafluoroborate is energetically unfavorable contrarily to the loss of HBF_4 which is documented in the literature for isolated coinage metal complexes containing BF_4^- counterions.[50]

At the CAM-B3LYP level, the partial charge on the complex metallic core is –0.570|e| for the $[\mathbf{1}\cdot(BF_4)_3]^+$ complex, –0.437|e| for the $[\mathbf{1}\cdot(BF_4)_2]^{2+}$ complex and –0.255|e| for the $[\mathbf{1}\cdot(BF_4)]^{3+}$ complex.

In what follows, all species of interest are mass-selected and isolated to achieve selective characterization of pure compounds.

Gas-phase photodissociation

The gas-phase photodissociation spectra of the $[\mathbf{1}\cdot(BF_4)_x]^{(4-x)+}$ and $[\mathbf{1}\cdot(BF_4)_{x-1}-H]^{(4-x)+}$ clusters (with $x=1$ and 2) are displayed in Figure 3. It was not possible to detect and analyze the $[\mathbf{1}\cdot(BF_4)_3]^+$ species due to the electrospray source and storage conditions of the setup employed for these investigations. We also note that the spectrum of the $[\mathbf{1}-H]^{3+}$ species (Figure 3-d) exhibits a poor signal-to-noise ratio, significantly worse than those of the other species and it is therefore only accessory to the present study.

A detailed analysis of the various photofragments is provided in the supplementary information (Figure S4, and Tables S1 and S2). The photofragmentation pathways of all four analyzed species range from neutral losses (charge retention) to ionic fragmentation (charge separation). Ionic fragmentation proceeds mainly via the cleavage of a $[Au(Dppy)_2]^+$ moiety while neutral loss photodissociation channels primarily encompass loss(es) of HBF_4 and/or loss(es) of $Dppy$ ligands.

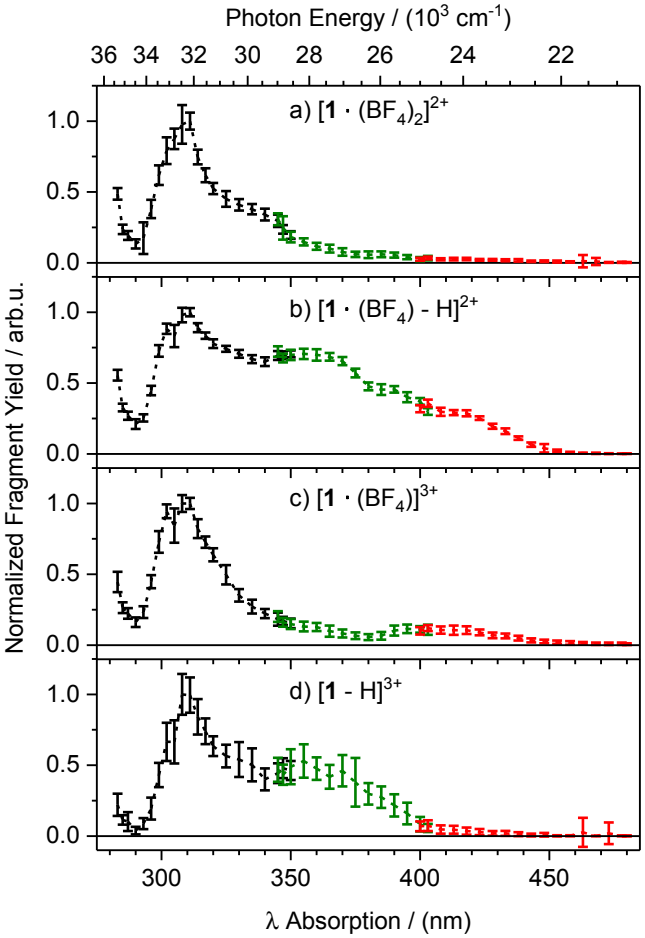

Figure 3. UV/Vis-photodissociation total yield spectra of gaseous precursor species a) m/z 1580, b) m/z 1536, c) m/z 1024, d) m/z 995 (nominal, 2μJ per pulse, 98 pulses per ion cloud). Color changes indicate a change in the nonlinear output scheme or wavelength filters requiring a re-optimization of the laser beam / ion cloud overlap. Error bars represent one standard deviation (±1σ, at least 160 mass spectra).

The following aspects determining the obtained photofragmentation yield are to be considered: the non-negligible heat capacity due to the respectable size of the clusters, the possible kinetic shifts pertaining to the dissociation,[51] and the competing quenching by helium inside the trap. Thus, the recorded photodissociation action spectra (Figure 3) do not directly reflect linear absorption spectra.[52] Moreover, the photofragment yield is only in the low laser fluence regime proportional to the oscillator strength and the quantum yield for dissociation. However, it was recently observed for Ru(II) complexes under ion trap conditions that gas-phase photodissociation action spectra display, albeit relatively weak electronic excitation bands at longer wavelengths comparable to solution absorption spectra.[53-54] Laser fluence-dependent measurements at 1-4 μJ per pulse were performed for selected spectral regions (see Figures S14-S17) displaying no significant dependence of spectral profiles on intensity and therefore ensure that the PD spectra were not measured under saturated conditions. Based on the observed non-linear increase of fragment yield upon doubling of the lase pulse energy (cf. Figure S15), the presumable large heat capacity of the cluster ions and the onset for HBF_4 loss at ~450 nm (266 kJ/mol), we assume the absorption of at least two photons prior to dissociation.

The experimental spectra obtained in this work nevertheless display a good agreement with computed data in the high energy spectral range (see next section). In particular, all investigated species (Figure 3-a-d) exhibit an absorption maximum at 310 nm

assigned in the next section to ^{1}LMCT transitions. This band can conveniently be used for the normalization of the photodissociation spectra as its computed intensity (see later on) does not significantly change for the different species. It should be emphasized that all spectra have been obtained under identical mass spectrometric and laser conditions (side-by-side measurements).

Interestingly, the photodissociation spectra of Figure 3 not only depend on the charge state but also on the number of associated tetrafluoroborates and the number of lost HBF_4 units. The $[\mathbf{1}\cdot(BF_4)_2]^{2+}$ species is the only one which also displays detectable luminescence in the gas phase upon excitation in the visible (at $\lambda_{ex}=$ 405, 458, and 476 nm) as discussed in the next section. While photoexcitation and photoluminescence excitation is possible using wavelengths longer than 400 nm, no absorption bands have been observed in the photodissociation spectrum of this species at $\lambda_{ex}>$ 400 nm (Figure 3-a). Moreover, its total fragmentation yield (TFY) is below 3% in this wavelength range in contrast to the $[\mathbf{1}\cdot(BF_4)-H]^{2+}$ and $[\mathbf{1}\cdot(BF_4)]^{3+}$ species. Since the other species, with the exception of $[\mathbf{1}\cdot(BF_4)]^{3+}$ which is not intense enough to be efficiently isolated and therefore investigated, were not found to lead to detectable photoluminescence under the conditions used, we propose that $[\mathbf{1}\cdot(BF_4)_2]^{2+}$ photoluminescence channels efficiently compete with photodissociation. While luminescence photoexcitation spectra could help to elucidate these competing processes involving the cluster excited states manifolds,[52] further support for this hypothesis also comes from the inspection of the photodissociation spectrum of the species $[\mathbf{1}\cdot(BF_4)]^{3+}$ (Figure 3-c). Its spectrum clearly displays a band centered about 415 nm comparable to the absorption spectra of $[\mathbf{1}](BF_4)_4$ in CH_2Cl_2.[28] Additionally, the increase of the TFY by a factor of 3-4 suggests that fragmentation-competing processes such as photoluminescence only play a minor role for this system. This behavior is consistent with the general idea that ions with higher overall charge are more susceptible to fragmentation than the ones of lower charge.

The $[\mathbf{1}\cdot(BF_4)-H]^{2+}$ cluster ion, whose structure we have not explored in the course of this work, shows a very high photofragment yield (Table 1) over the whole spectral range (Figure 3-b). Its photodissociation spectrum gives evidence for absorption bands up to 460 nm. Its high reactivity probably originates from the activated/high energy structure of the ligand moiety formed after formal loss of a proton with the HBF_4 leaving group. This high fragment yield of $[\mathbf{1}\cdot(BF_4)-H]^{2+}$ is in accordance with our finding (see below) that photoluminescence was not detectable for this species.

Upon comparison of the PD spectra of cluster species differing by the loss of a neutral HBF_4 moiety (Figure 3, a) vs b); c) vs d)), pronounced spectral differences in the range of 320-450 nm are evident, whose assignments would require more detailed quantum-chemical calculations which are beyond the scope of this paper. Presumably, loss of HBF_4 should result in change of the charge density and/or charge density distribution of the $[(C)Au_6Ag_2]$ metal core or radical character located at the dehydrogenated ligands, leading to new electronic states and coupling.

The channel-specific spectra are provided in the supporting information (see Figs. S7-S10) and display a very similar shape compared to the total yield spectra suggesting that the excess energy is presumably statistically distributed in all (mostly vibrational) degrees-of-freedom (ergodic fragmentation). There is no indication of state-specific fragmentation.

Table 1. Total fragment yields and photoluminescence features for $[\mathbf{1}\cdot(\boldsymbol{BF_4})_x]^{(4-x)+}$ and $[\mathbf{1}\cdot(\boldsymbol{BF_4})_{x-1}-\boldsymbol{H}]^{(4-x)+}$ cluster species (with $x=$ 1 and 2).

Species	m/z nominal	m/z Main isotopolog.	Photodissociation Total frag. yield/% @308nm	@408nm	Photoluminescence λ_{em}/nm λ_{ex}=405nm
$[\mathbf{1}\cdot(BF_4)_2]^{2+}$	1580	1581.06	44	2	~677 (Phos.)
$[\mathbf{1}\cdot(BF_4)-H]^{2+}$	1536	1537.06	72	26	- *
$[\mathbf{1}\cdot(BF_4)]^{3+}$	1024	1025.04	64	8	- *
$[\mathbf{1}-H]^{3+}$	995	995.70	27	2	not investigated
$[\mathbf{1}\cdot(BF_4)_3]^{+}$	3247	3249.13	-	-	~673 (Phos.), ~586

* no detectable photoluminescence.

Gas-phase photoluminescence

Gas-phase photoexcitation of the $[\mathbf{1}\cdot(BF_4)_x]^{(4-x)+}$ clusters was found to lead to detectable emission upon excitation at $\lambda_{ex}=$ 405, 458, and 476 nm only for the mono and doubly charged species, with $x=$ 3 and 2, respectively. Although $[\mathbf{1}\cdot(BF_4)]^{3+}$ could not be unambiguously isolated on the photoluminescence setup, based on the absorption spectra of Figure 3, the absence of detectable emission for the abundant $[\mathbf{1}-H]^{3+}$ trication suggests an increase in the efficiency of the non-radiative, probably fragmentation, channels or a reduction of the absorption cross-section as the overall charge of the cluster increases (as the number of tetrafluoroborates decreases). At threshold excitation, when no fragmentation occurs, the $[\mathbf{1}\cdot(BF_4)_3]^{+}$ monocation and the $[\mathbf{1}\cdot(BF_4)_2]^{2+}$ dication have close to identical emission profile (Figures 4 and S5). The apparent dual emission observed for the $[\mathbf{1}\cdot(BF_4)_3]^{+}$ monocations ($\lambda_{ex}=$ 405 nm) with the lower energy component at close to the same position as the dication (673 versus 677 nm) and a high energy component (at 586 nm) shifted to the blue by 87 nm (2200 cm^{-1}) appears to result from intersystem crossing to the triplet state and a fragmentation process induced by the excess energy deposited on the cluster.

Lifetime measurements (Figure 5) were performed in order to gain information on the nature of the transitions involved and rule out fluorescence concomitant to phosphorescence. While the onset of the photoluminescence signal is related to the population of the emitting state (including the impact of ion motion and overlap between the excitation beam and the ion cloud), the photoluminescence decays (for the spectrally integrated luminescence) are mono-exponential, independent of the irradiance used, and give respective lifetime values of $20.4\pm0.5\,\mu s$ and $21.4\pm0.6\,\mu s$ for the $[\mathbf{1}\cdot(BF_4)_3]^{+}$ and $[\mathbf{1}\cdot(BF_4)_2]^{2+}$ clusters, consistent with phosphorescence emission.

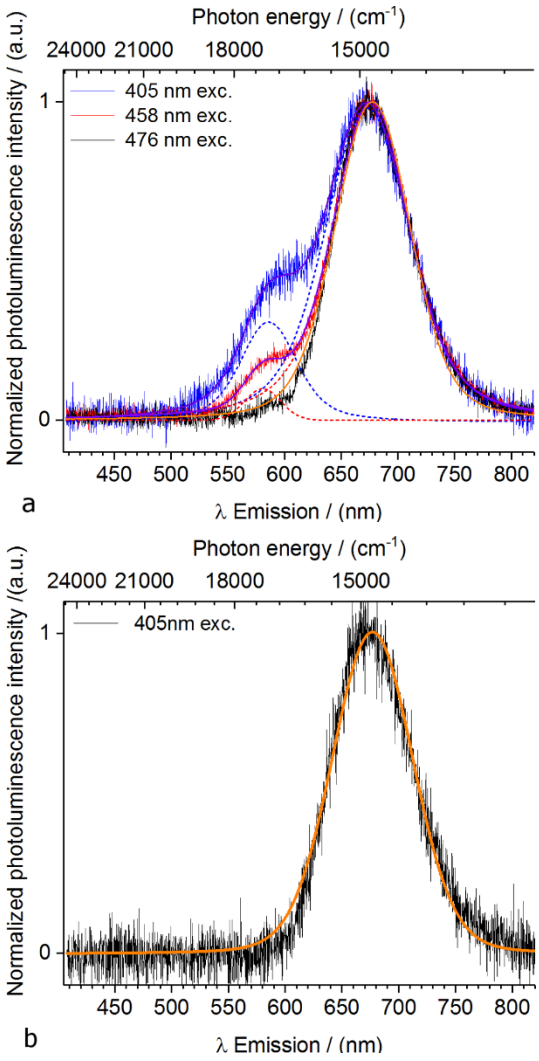

Figure 4. Emission spectra of the a) $[\mathbf{1}\cdot(BF_4)_3]^+$ and b) $[\mathbf{1}\cdot(BF_4)_2]^{2+}$ species for ions stored in a Paul trap at 83 K. The spectra taken at excitation wavelengths of 405, 458, and 476 nm being similar, only the spectrum taken at 405 nm is displayed for the dication. The spectra have been fitted using Voigt profiles (fits given as solid lines and components as dashed lines). Irradiances 300 W/cm^2 (405 nm), 675 W/cm^2 (458 nm), and 750 W/cm^2 (476 nm).

The fragment origin of the shoulder observed in Figure 4-a is supported by the photoluminescence of the m/z 2700 photo-fragment, $[\mathbf{1}\cdot(BF_4)-Ag-Dppy-2.H]^+$, (Figure S6). This fragment is not ejected from the trap while recording the emission of the $[\mathbf{1}\cdot(BF_4)_3]^+$ species due to a necessary tradeoff: high buffer gas pressure is needed to prevent fragmentation; cw excitation intensity cannot be reduced beyond a threshold (system dependent) due to limited emitted light collection efficiency (~0.6%); increasing the low mass cutoff at a fixed angular frequency (300 kHz for the trap used) implies increasing the amplitude V of the rf-potential; and going beyond the value of V = 1090V on the setup used (q_z=0.46 for the m/z 3248 species) leads to the formation of a helium plasma in the trap. Furthermore, while the coexistence of isomers is in principle possible, there is no evidence of isomers in the ion mobility measurements performed on the ions in their ground state. Consequently, the m/z 2700 species generated upon photo-fragmentation and co-trapped with the monocations of interest is most likely responsible for the shoulder observed in Figure 4-a.

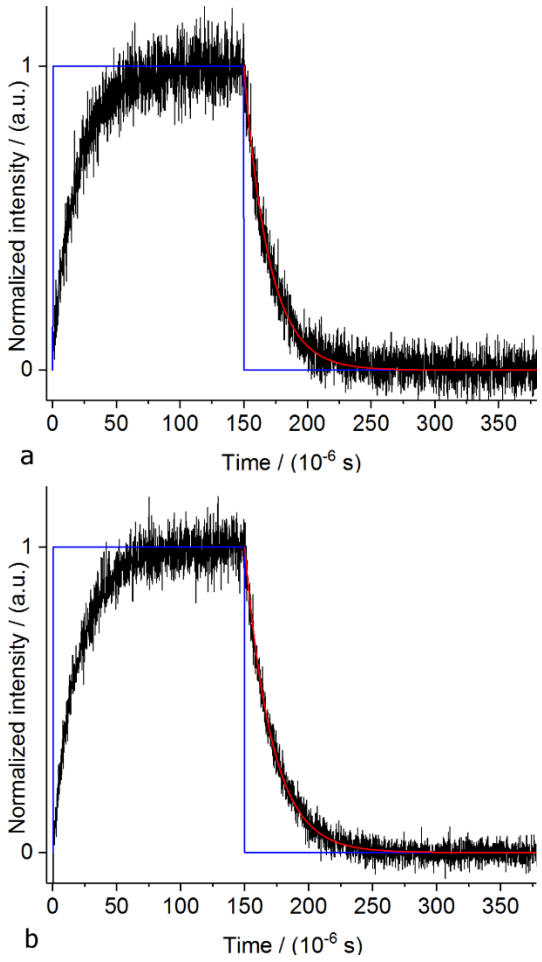

Figure 5. Lifetime measurements for a) $[\mathbf{1}\cdot(BF_4)_3]^+$ (405 nm, 80 W/cm^2) $\tau = 20.4 \pm 0.5\ \mu s$ and b) $[\mathbf{1}\cdot(BF_4)_2]^{2+}$ (405 nm, 380 W/cm^2) $\tau = 21.4 \pm 0.6\ \mu s$ molecular cluster cations. The blue line corresponds to the time the laser is on. Once stationarity has been achieved the laser is turned off and photoluminescence decay measured.

Computations on electronically excites states and comparison to experimental results

Insight into the structural and electronic changes undergone by the $[\mathbf{1}\cdot(BF_4)_x]^{(4-x)+}$ gas-phase species as the overall charge of the cluster increases is provided by density functional calculations. The structures of the $[\mathbf{1}\cdot(BF_4)_3]^+$ and $[\mathbf{1}\cdot(BF_4)_2]^{2+}$ computed at the CAM-B3LYP level (see Figure 2-c,d) and shortly described before are characterized by bond lengths between the central carbon and the Au atoms of 2.162 ± 0.046 Å and 2.164 ± 0.047 Å, respectively. Each Au· · ·Ag edge is bridged by one *Dppy* ligand with the P atom bound to Au (2.344 ± 0.074 Å and 2.347 ± 0.078 Å, respectively) and the pyridyl N atom coordinated to Ag (2.457 ± 0.103 Å and 2.455 ± 0.097 Å, respectively) conferring together with the Au· · ·Ag metallophilic interactions (3.078 ± 0.201 Å and 2.993 ± 0.081 Å, respectively) extra rigidity. Overall values inferred from the computations on charged structures and crystallographic values for the neutral species[32] are found to be in good agreement. The gas-phase computed ground state equilibrium structures retain the "capped sphere" structural motif and bond lengths are systematically longer than those of the crystallographic structure, the changes in structural parameters being on the order of 0.1 Å. The elongation of the Au· · ·C, Au· · ·Au, Ag· · ·C and Ag· · ·N distances is expected when going from a crystallographic structure to a gas-phase equilibrium geometry

for which there is no crystal "pressure". In the lowest-lying triplet state, the "capped sphere" structural motif and cluster are perturbed but the Au· · ·Ag and Au· · ·P distances show no or only minor changes compared to the singlet ground state.

The cluster equilibrium geometry, two $AgAu_3(Dppy)_3$ units bridged by a carbon atom, favors triplet states with a high luminescence quantum yield[55] as evidenced by the emission band reported for the $[\mathbf{1}\cdot(BF_4)_4]$ solubilized in CH_2Cl_2 and found to be between 600 nm[32] and 640 nm.[28] This band has been previously assigned to phosphorescence from a low-lying spin-forbidden excited state due to its significant red shift from the absorption onset (at 485 nm in CH_2Cl_2) and long lifetime ($\tau_0 = 4.7\ \mu s$ in CH_2Cl_2).[28] The gas-phase luminescence lifetimes, being about 20 μs for the $[\mathbf{1}\cdot(BF_4)_3]^+$ and $[\mathbf{1}\cdot(BF_4)_2]^{2+}$ species, are similarly ascribed to phosphorescence (see below). Furthermore, the solution absorption band position displays a hypsochromic (blue) shift of approximately 10 nm when the solvent is changed from CH_2Cl_2 or CH_3CN to CH_3OH, while a larger (> 35 nm) red-shift is observed in the gas phase compared to solution measurements. Due to the shielding of the gold-core from the environment by the ligands (see Figure S7 for a space filling representation), it appears likely that this gas-phase red shift compared to solution is caused by solvent interactions either stabilizing a ligand-centered ground state (in the case of a ^{3}MLCT transition), destabilizing a ligand-centered excited state (in the case of a ^{3}LMCT), or is induced by the number of counterions bound in solution. The featureless gas-phase emission bands also display characteristics typical of metal centered (MC) transitions as discussed hereafter with the support of TD-DFT computations.

The nature of the electronic states involved in the gas-phase photoluminescence of the $[\mathbf{1}\cdot(BF_4)_3]^+$ and $[\mathbf{1}\cdot(BF_4)_2]^{2+}$ species has been investigated at the TD-DFT CAM-B3LYP computational level. Mainly, two types of transitions can be distinguished in the absorption and emission spectra of the species studied. On the one hand, there are excitations involving molecular orbitals "purely" localized on the metallic core (Figure 6). On the other hand, there are excitations between core localized and ligand localized MO that yield electron charge transfer from the metallic core to the ligands (MLCT) or reciprocally (LMCT).

The three HOMO, HOMO − 1, HOMO – 2 orbitals of the $[\mathbf{1}\cdot(BF_4)_3]^+$ cluster are nearly degenerate and mainly consist of Au core orbitals (see supporting information, Figure S8). They correspond to a set of superatomic p orbitals[56] localized on the cluster core. The LUMO resembles a superatomic d orbital delocalized on the Au core split by more than 2.3 eV from the other much higher in energy d-like superatomic orbitals. The LUMO+1 up to LUMO+6 MO's, on the other hand, are preferably localized on the $Dppy$ ligand shell. A representation of the main MO's involved in the optical transitions of the $[\mathbf{1}\cdot(BF_4)_3]^+$ cluster is displayed in Figure 6-a.

The highest occupied and lowest unoccupied MO's of the $[\mathbf{1}\cdot(BF_4)_2]^{2+}$ cluster are very similar to those of $[\mathbf{1}\cdot(BF_4)_3]^+$ cluster (see supporting information, Figure S9). The three highest occupied MO's of the $[\mathbf{1}\cdot(BF_4)_2]^{2+}$ cluster mainly consist of Au core orbitals with a superatomic p character[56] while the core-centered superatomic d-like LUMO is separated from similar d-like orbitals by more than 5 eV and the LUMO+1 to LUMO+6 MO's are delocalized on the $Dppy$ surface ligands, as displayed in Figure 6-b.

The shifted computed absorption and emission spectra of $[\mathbf{1}\cdot(BF_4)_3]^+$ are displayed in Figure 7-a,b. The computed absorption and emission profiles have been respectively red shifted in energy by 0.682 eV in (a) and 0.701 eV in (c) and blue shifted in energy by 0.536 eV in (b) and 0.265 eV in (d) in order to match the main features of the experimental photodissociation and photoluminescence spectra. For the absorption, the onset of the 310 nm band shared by all species (see Figure 3) and assumed to be similar for the $[(C)(AuDppy)_6Ag_2\cdot(BF_4)_3]^+$ monocation was taken as reference while for the emission the parameters were adjusted such as to match the observed triplet emission. The absorption spectrum of $[\mathbf{1}\cdot(BF_4)_3]^+$ (Figure 7-a) shows multiple molecule-like singlet-type bands at 420, 334, 303, and 275 nm associated with core-centered as well as metal-to-ligand charge transfer (^{1}MLCT) transitions. The low energy tail explains photoexcitation in the visible range up to 476 nm. The computed emission spectrum of Figure 7-b displays multiple bands corresponding to 1) experimentally unobserved excited singlet fluorescence (556, 442, and 393 nm, orange line) with the weak 556 and 442 nm bands corresponding to core-centered transitions while the peak at 393 nm corresponds to a ligand-to-metal charge transfer transition, 2) mostly metal-centered lowest triplet state phosphorescence (678 nm, green line), and 3) excited triplet-triplet emission (about 672, 614, and 522 nm, blue line) associated with ligand-to-metal charge transfer (LMCT) transitions in all three cases. Only a single intense phosphorescent transition was found computationally (Figure 7-b, green line), which agrees with the simple luminescent band profile measured experimentally. Accordingly, an energy diagram is provided in Figure 8.

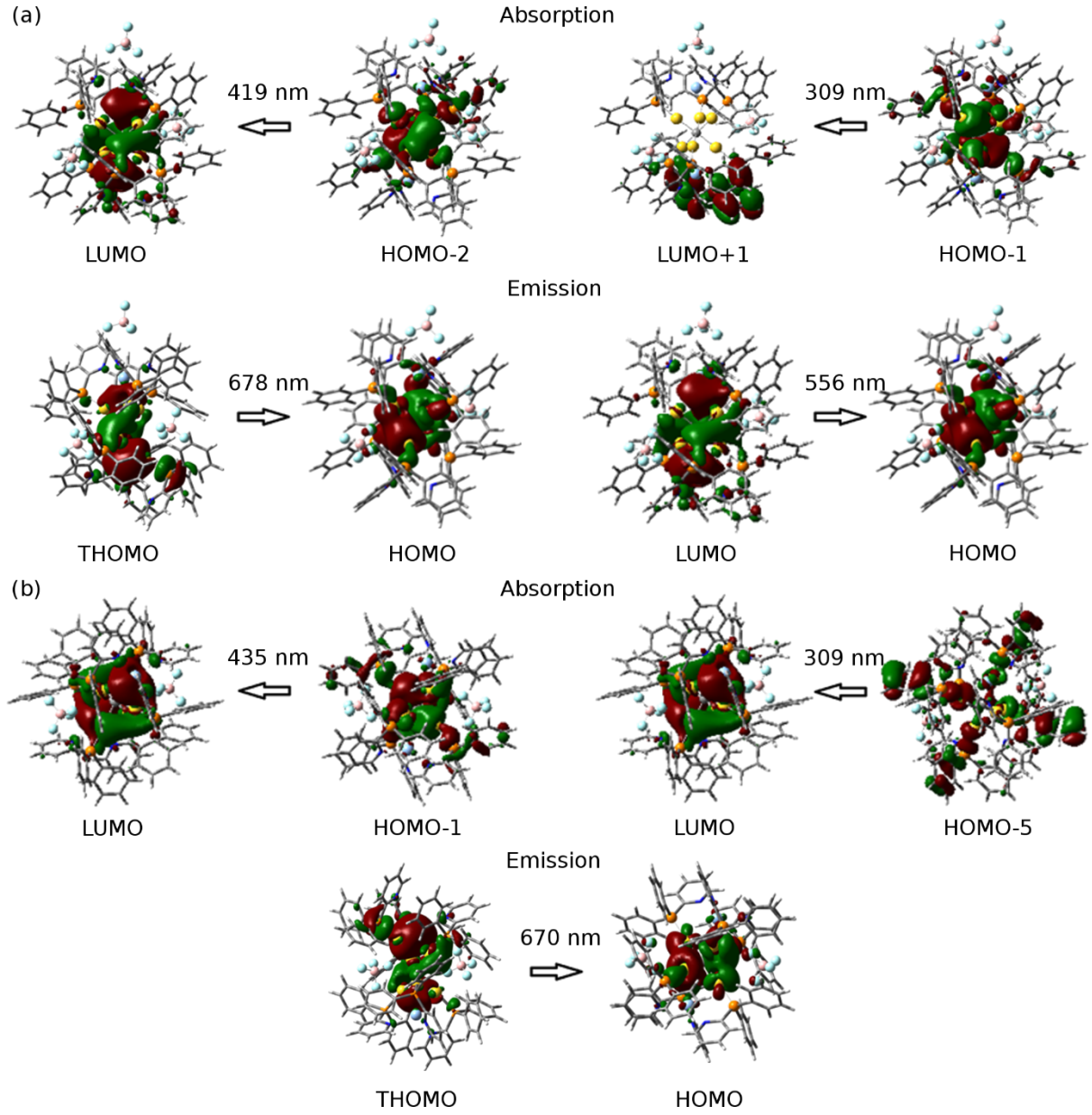

Figure 6. Representation of the main orbitals involved in the optical transitions of (a) $[\mathbf{1}\cdot(BF_4)_3]^+$ and (b) $[\mathbf{1}\cdot(BF_4)_2]^{2+}$. The MO's involved in the excitation of the electronic states leading to the absorption and emission spectra are separately represented. Emission mainly comes from the lowest triplet state with singly occupied molecular orbitals (THOMO).

The shifted computed absorption and emission spectra of $[\mathbf{1}\cdot(BF_4)_2]^{2+}$ are plotted in Figure 7-c,d. The absorption spectrum (Figure 7-c) shows multiple molecule-like bands at 434, 337, 297, and 274 nm associated with core-centered and metal-to-ligand charge transfer (^{1}MLCT) transitions. Once again the low energy tail explains the experimentally observed excitation up to 476 nm. The marked difference around 420 nm between the absorption spectrum computed for the $[\mathbf{1}\cdot(BF_4)_2]^{2+}$ species and the photodissociation spectrum (Figure 7-c) is, as previously mentioned, likely due to the effectively competing radiative (photoluminescence) channel: the emitted energy being unavailable for fragmentation. It should be noted that the solution (CH_2Cl_2) absorption spectrum of $[\mathbf{1}](BF_4)_4$ also exhibits a broad, although weak, band in the 380-470 nm region.[28]

The computed emission spectrum of Figure 7-d corresponds to 1) experimentally unobserved singlet-type fluorescence bands significantly blue shifted compared to the $[\mathbf{1}\cdot(BF_4)_3]^+$ cluster (orange line). Of those, only the 470 nm singlet-type fluorescence band corresponding to a core-centered transition involving fluorescence from the lowest excited singlet state is visible in the computed spectrum (the other bands being significantly higher in energy), 2) a mostly core-centered triplet phosphorescence band at 677 nm (green line) used as in the previous case as reference for the computed spectra, and 3) multiple excited triplet-triplet emission band (659, 575, 486, and 460 nm band, blue line) associated with ligand-to-metal charge transfer (LMCT) transitions. Overall, the single intense phosphorescent transition calculated for $[\mathbf{1}\cdot(BF_4)_2]^{2+}$ (Figure 7-d) agrees well with the experimental one suggesting that only the triplet phosphorescence band is experimentally observed. A summarizing energy diagram is provided in Figure 8.

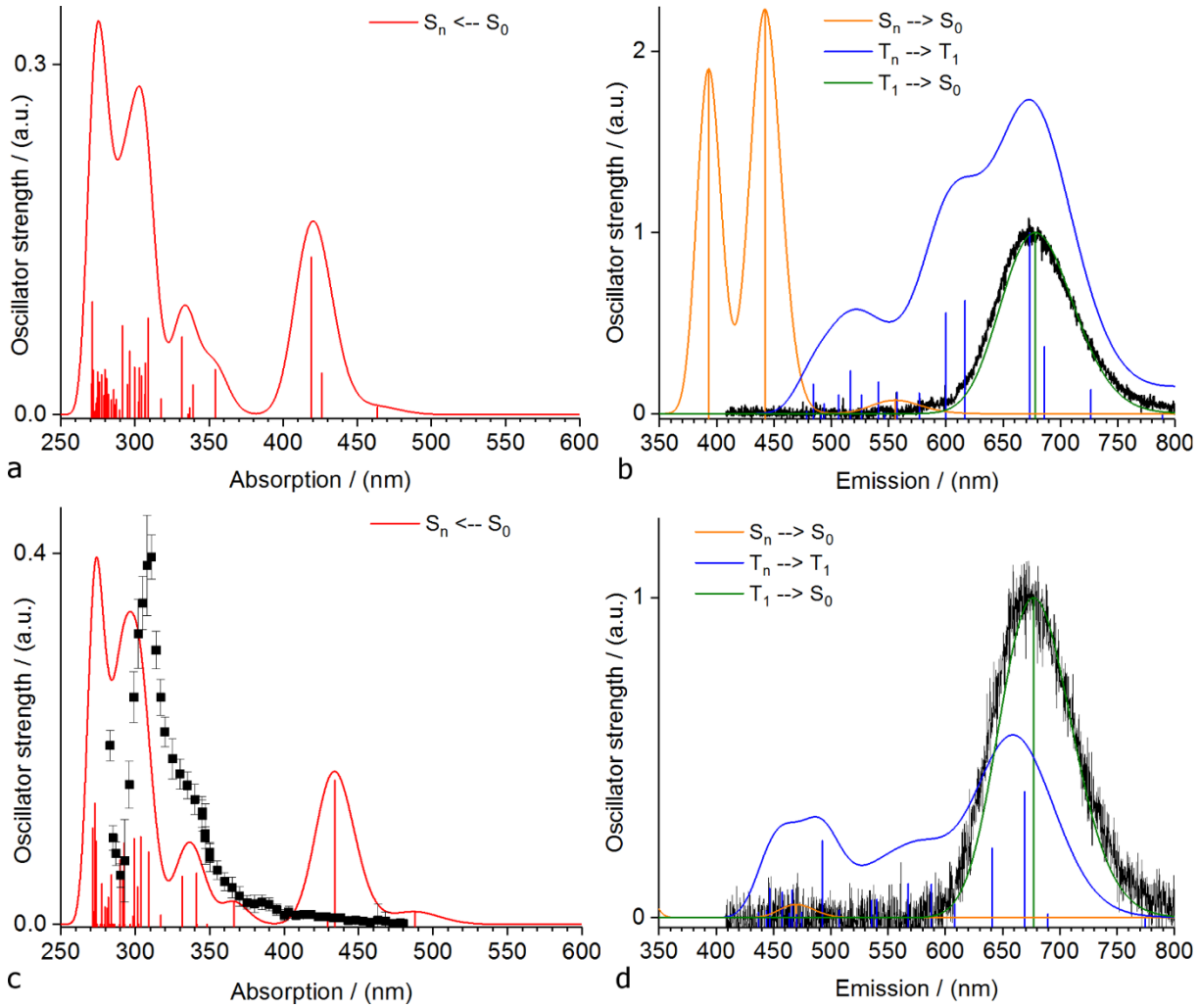

Figure 7. Computed absorption (left) and emission (right) spectra of (a-b) $[\mathbf{1}\cdot(BF_4)_3]^+$ and (c-d) $[\mathbf{1}\cdot(BF_4)_2]^{2+}$ at the TD-DFT CAM-B3LYP level. Absorption profiles (red) are obtained at the equilibrium geometry of the S_0 state and spectrum convolution has been done using Gaussian functions with variance σ =0.085 eV. Emission spectra are computed at the equilibrium geometry of the S_1 and T_1 states. The computed absorption and emission profiles have been respectively red shifted in energy by 0.682 eV in (a) and 0.701 eV in (c) and blue shifted in energy by 0.536 eV in (b) and 0.265 eV in (d) in order to match the main features of the experimental photodissociation and photoluminescence spectra (see text). The gas-phase experimental data is displayed in black. The accuracy of computed excitation energies at the TD-DFT level is expected to be about 0.5 to 1 eV, depending on the character of the excited states.

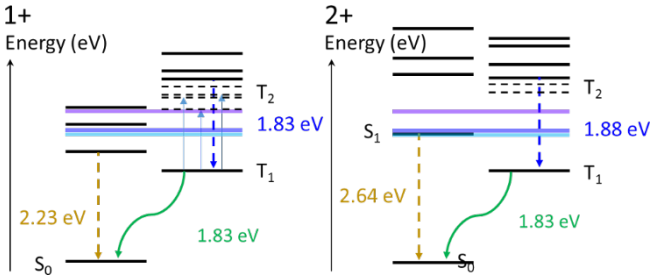

Figure 8. Semi-quantitative energy diagram of the lowest-energy levels involved in the emission spectrum of the $[\mathbf{1}\cdot(BF_4)_3]^+$ cluster (1+) and the $[\mathbf{1}\cdot(BF_4)_2]^{2+}$ cluster (2+) adjusted to experimental data. Orange lines correspond to decay from the lowest excited singlet state while dashed blue lines describe transitions to the lowest excited triplet state. Solid green lines are associated to phosphorescence from the "ground state" triplet to the ground state singlet. The dashed levels correspond to the excited triplet states involved in the lowest energy transition lines of Figure 7-b,d. The horizontal colored lines corresponds to the excitation energies (light blue 476 nm, dark blue 458 nm, and purple 405 nm).

In summary, the low energy peak at about 675 nm of Figure 7 shared by both the $[\mathbf{1}\cdot(BF_4)_3]^+$ and $[\mathbf{1}\cdot(BF_4)_2]^{2+}$ species is clearly identified as mostly-core-centered phosphorescence from the lowest energy triplet state while the high energy component of $[\mathbf{1}\cdot(BF_4)_3]^+$ emission corresponds to the emission from fragments. Unfortunately, we could not unambiguously identify the fragment ions responsible. We presume, however, that they are formed by loss of one or both capping Ag of the Au_6Ag_2 cluster unit, because it was reported that $[(C)(AuDppy)_6](BF_4)_2$ exhibits blue-shifted luminescence ($\lambda_{em}\approx$ 440 nm) in CH_2Cl_2 solution compared to $[\mathbf{1}](BF_4)_4$ ($\lambda_{em}\approx$ 600 nm).[32] As displayed in Figure 8, the lowest energy triplet (T_1) – S_0 energy gap is about 1.83 eV and the excited triplet (T_2) – lowest energy triplet (T_1) gap is at least 1 eV. An alternative explanation to the emission spectra involving fluorescence inside the triplet manifold – it would imply the population of an excited triplet state via a (sequential) two photon excitation likely requiring much higher irradiances than the ones used here – is ruled out based on luminescence lifetimes. A study involving time-resolved (as well as irradiance dependent)

measurements will be reported elsewhere. Interestingly dual luminescence in the green and orange-red regions has also been observed in assemblies of discrete molecular decanuclear gold(I) sulfido complexes.[57] The high-energy emission with a comparatively smaller intensity has been ascribed in these systems to a metal-perturbed intra-ligand phosphorescence while the low-energy emission was tentatively assigned either to emission from triplet states with a ligand-to-metal charge transfer (^{3}LMCT) or metal/core-based (ds/dp) character.[57]

Overall, many photophysical properties of the lowest excited states and corresponding transitions of organometallic compounds are determined by the extent of metal participation in the excited state wavefunctions. This metal participation not only alters their spatial extension, but also induces significant mixtures of singlet and triplet states by spin-orbit coupling.[58] Additionally the solvent significantly affects charge transfer processes characterized by a substantial change in electronic distribution between the initial and final states. The surrounding solvent molecules responding to this change can substantially influence the electron transfer rate as well as cause significant shifts in absorption or emission.[59] Accordingly, the present work provides valuable information about both excited states and intramolecular charge transfer processes, which underlie numerous conversions of light into chemical, electrical, and/or mechanical energy, by enabling characterization in the absence of polarizable medium and proton translocation.[59] Differences are highlighted with solution data. According to Ref. 28, the 405 nm excitation of the solvated $[\mathbf{1}\cdot(BF_4)_4]$ species – the computations of Ref. 28 were performed on the $[\mathbf{1}]^{4+}$ ion – selectively (though not solely) populate the surface ligand states and correspond to a ^{1}MLCT transition between Au(I) and surface ligands in solution resulting in a single emission band with ^{3}MLCT character. In the gas phase, while the process is essentially the same, the excess energy deposited on the $[\mathbf{1}\cdot(BF_4)_3]^+$ cluster upon 405 nm excitation (the emission is red-shifted by about 35 nm compared to solution data) as well as intersystem crossing to the triplet state, leads to fragmentation as evidenced from the observed dual emission. Since the same observation is not made for the $[\mathbf{1}\cdot(BF_4)_2]^{2+}$ species, it is suggested that the interpretation of the solution results may be complicated by superposition effects.

CONCLUSION

In summary, the experimental and computational results reported here suggest that the main luminescence band of the $[\mathbf{1}\cdot(BF_4)_x]^{(4-x)+}$ species originates from low lying mostly-core-centered localized triplet states. Using gas-phase measurements on mass selected ions we have enabled direct comparison with computations and thereby considerably simplified the analysis. Gas-phase excitation at 476 nm (and 83 K) is found to involve a transition between states localized at the cluster core and the ligand shell, followed by intersystem crossing to the triplet manifold and a core-centered emission from a mostly core-centered state. Dual emission is observed for the $[\mathbf{1}\cdot(BF_4)_3]^+$ species upon 405 nm excitation (at 83 K). This is rationalized by the fragmentation of the observed species (supposedly forming an entity without capping Ag) when the energy deposited upon excitation is sufficient for dissociation. Interestingly, while the computed results concur with the limited photoexcitation data, the photodissociation spectra were found to highlight non-radiative, i.e. fragmenting processes or the absence thereof, complementary to the observation of photoluminescence.

Consequently, the present work provides a deeper understanding of the nature of the optical transitions, the impact of tetrafluoroborates on these transitions, as well as a better understanding of the environment dependence of ultrasmall gold clusters' photophysical properties. It may thereby contribute to the rational design of tunable ligand protected gold clusters with a fast and efficient intersystem crossing (ISC) from the excited singlet to the light emitting triplet states for application as emitters and sensors. In particular, the present work suggests a systematic study of counterions effects may help optimize properties with ion trap experiments playing a decisive role for these studies. We have demonstrated here, that the isolation and separate spectroscopic investigation of different counterion adducts is feasible by this technique so that unprecedented insights into details of microsolvation and also their ultrafast dynamics are within reach.

ASSOCIATED CONTENT

Supporting Information

Mass spectrum, comparison of $[\mathbf{1}\ .\ (BF_4)_3]^+$ and $[\mathbf{1}\ .\ (BF_4)_2]^{2+}$ isomers, unpaired electron density for $[\mathbf{1}]^{3+}$, PD mass spectra, Channel-specific PD spectra, Photofragments assignments, Comparison emission spectra of $[\mathbf{1}\cdot(BF_4)_3]^+$ and $[\mathbf{1}\cdot(BF_4)_2]^{2+}$, Photoluminescence spectrum of m/z 2700 fragment, Space filling representation of the $[\mathbf{1}\cdot(BF_4)_3]^+$ cluster, MO energy diagram of $[\mathbf{1}\ .\ (BF_4)_3]^+$ and $[\mathbf{1}\ .\ (BF_4)_2]^{2+}$, Channel specific PD spectra, PD total yields. This material is available free of charge via the Internet at http://pubs.acs.org.

AUTHOR INFORMATION

Corresponding Author

j.greisch@uu.nl

Present Addresses

† Utrecht University, Hecklab, Padualaan 8, 3584CH, Utrecht, The Netherlands.

Notes

The authors declare no competing financial interests.

ACKNOWLEDGMENT

This work has been supported by the Deutsche Forschungsgemeinschaft (DFG) through CRC/TRR 88 „Cooperative Effects in Homo- and Hetero-metallic Complexes (3MET)“ (Projects C4 and C7). J.-F.G. acknowledges support from the Hector Fellow Academy (HFA) and would like to express his deepest thanks to Prof. Manfred M. Kappes and PD Dr. Detlef Schooss for fruitful discussions. A.B.-G. acknowledges the University of Liege and the EU in the context of the MSCA-COFUND-BeIPD project. F.R. acknowledges the Fonds de la Recherche Fondamentale Collective (FRFC 2.5020.11) for computational resources and Fonds National de la Recherche Scientifique (FRS-FRNS) for its support. The Bundesministerium für Bildung und Forschung (BMBF) through the Helmholtz Research Program POF Science and Technology of Nano-systems is also acknowledged by J.-F.G. for support and for providing the necessary infrastructure.

REFERENCES

1. Wang, Q. M.; Lee, Y. A.; Crespo, O.; Deaton, J.; Tang, C.; Gysling, H. J.; Gimeno, M. C.; Larraz, C.; Villacampa, M. D.; Laguna, A. *et al.*, Intensely Luminescent Gold(I) - Silver(I) Cluster Complexes with Tunable Structural Features. *J. Am. Chem. Soc.* **2004,** *126*, 9488-9489.

2. Yam, V. W. W.; Cheng, E. C. C., Highlights on the Recent Advances in Gold Chemistry—a Photophysical Perspective. *Chem. Soc. Rev.* **2008,** *37*, 1806-1813.
3. Whetten, R. L.; Shafigullin, M. N.; Khoury, J. T.; Schaaff, T. G.; Vezmar, I.; Alvarez, M. M.; Wilkinson, A., Crystal Structures of Molecular Gold Nanocrystal Arrays. *Acc. Chem. Res.* **1999,** *32*, 397-406.
4. Jin, R., Quantum Sized, Thiolate-Protected Gold Nanoclusters. *Nanoscale* **2010,** *2*, 343-362.
5. Templeton, A. C.; Wuelfing, W. P.; Murray, R. W., Monolayer Protected Cluster Molecules. *Acc. Chem. Res.* **1999,** *33*, 27-36.
6. Chen, Y. S.; Kamat, P. V., Glutathione-Capped Gold Nanoclusters as Photosensitizers. Visible Light-Induced Hydrogen Generation in Neutral Water. *J. Am. Chem. Soc.* **2014,** *136*, 6075-6082.
7. Chen, Y. S.; Choi, H.; Kamat, P. V., Metal-Cluster-Sensitized Solar Cells. A New Class of Thiolated Gold Sensitizers Delivering Efficiency Greater Than 2%. *J. Am. Chem. Soc.* **2013,** *135*, 8822-8825.
8. Lei, Z.; Pei, X.-L.; Jiang, Z.-G.; Wang, Q.-M., Cluster Linker Approach: Preparation of a Luminescent Porous Framework with NbO Topology by Linking Silver Ions with Gold(I) Clusters. *Angew. Chem. Int. Ed.* **2014,** *53*, 12771−12775.
9. Chen, M.; Lei, Z.; Feng, W.; Li, C.; Wang, Q. M.; Li, F., A Phosphorescent Silver(I)-Gold (I) Cluster Complex that Specifically Lights up the Nucleolus of Living Cells with FLIM Imaging. *Biomaterials* **2013,** *34*, 4284-4295.
10. Weiss, D. N.; Brokmann, X.; Calvet, L. E.; Kastner, M. A.; Bawendi, M. G., Multi-Island Single-Electron Devices from Self-assembled Colloidal Nanocrystal Chains. *Appl. Phys. Lett.* **2006,** *88*, 143507.
11. Cheng, E. C. C.; Lo, W. Y.; Lee, T. K. M.; Zhu, N.; Yam, V. W. W., Synthesis, Characterization, and Luminescence Studies of Discrete Polynuclear Gold(I) Sulfido and Selenido Complexes with Intramolecular Aurophilic Contacts. *Inorg. Chem.* **2014,** *53*, 3854-3863.
12. Yao, L. Y.; Hau, F. K. W.; Yam, V. W. W., Addition Reaction-Induced Cluster-to-Cluster Transformation: Controlled Self-Assembly of Luminescent Polynuclear Gold(I) μ3□Sulfido Clusters. *J. Am. Chem. Soc.* **2014,** *136*, 10801-10806.
13. Lee, T. K. M.; Zhu, N.; Yam, V. W. W., An Unprecedented Luminescent Polynuclear Gold(I) μ3-Sulfido Cluster With a Thiacrown-like Architecture. *J. Am. Chem. Soc.* **2010,** *132*, 17646-17648.
14. Cunningham, A.; Mühlig, S.; Rockstuhl, C.; Bürgi, T., Coupling of Plasmon Resonances in Tunable Layered Arrays of Gold Nanoparticles. *J. Phys. Chem. C* **2011,** *115*, 8955-8960.
15. Mühlig, S.; Cunningham, A.; Scheeler, S.; Pacholski, C.; Bürgi, T.; Rockstuhl, C.; Lederer, F., Self-Assembled Plasmonic Core Shell Clusters with an Isotropic Magnetic Dipole Response in the Visible Range. *ACS Nano* **2011,** *5*, 6586-6592.
16. Evans, R. C.; Douglas, P.; Winscom, C. J., Coordination Complexes Exhibiting Room-temperature Phosphorescence: Evaluation of their Suitability as Triplet Emitters in Organic Light Emitting Diodes. *Coord. Chem. Rev.* **2006,** *250*, 2093-2126.
17. Pyykkö, P., Strong Closed-Shell Interactions in Inorganic Chemistry. *Chem. Rev.* **1997,** *97*, 597-636.
18. Pyykkö, P., Theoretical Chemistry of Gold. *Angew. Chem. Int. Ed.* **2004,** *43*, 4412-4456.
19. Schmidbaur, H., Ludwig Mond Lecture. High-carat gold compounds. *Chem. Soc. Rev.* **1995,** *24*, 391-400.
20. Schmidbaur, H., The Fascinating Implications of New Results in Gold Chemistry. *Gold Bull.* **1990,** *23*, 11-21.
21. Li, Q.; Li, H.; Li, R.; Jing, B.; Liu, Z.; Li, W.; Luan, F.; Cheng, J.; Gong, B.; Sun, J., Influence of Hybridization and Cooperativity on the Properties of Au-Bonding Interaction: Comparison with Hydrogen Bonds. *J. Phys. Chem. A* **2011,** *115*, 2853-2858.
22. Ingram, R. S.; Hostetler, M. J.; Murray, R. W.; Schaaff, T. G.; Khoury, J. T.; Whetten, R. L.; Bigioni, T. P.; Guthrie, D. K.; First, P. N., 28 kDa Alkanethiolate-Protected Au Clusters Give Analogous Solution Electrochemistry and STM Coulomb Staircases. *J. Am. Chem. Soc. 119*, 9279-9280.
23. Chen, S.; Ingram, R. S.; Hostetler, M. J.; Pietron, J. J.; Murray, R. W.; Schaaff, T. G.; Khoury, J. T.; Alvarez, M. M.; Whetten, R. L., Gold Nanoelectrodes of Varied Size: Transition to Molecule-Like Charging. *Science* **1998,** *280*, 2098-2101.
24. Negishi, Y.; Nobusada, K.; Tsukuda, T., Glutathione-Protected Gold Clusters Revisited: Bridging the Gap between Gold(I)-Thiolate Complexes and Thiolate-Protected Gold Nanocrystals. *J. Am. Chem. Soc.* **2005,** *127*, 5261–5270.
25. Green, T. D.; Knappenberger, K. L. J., Relaxation Dynamics of $Au_{25}L_{18}$ Nanoclusters Studied by Femtosecond Time-resolved near Infrared Transient Absorption Spectroscopy. *Nanoscale* **2012,** *4*, 4111-4118.
26. Muñiz, J.; Wang, C. R.; Pyykkö, P., Aurophilicity: The Effect of the Neutral Ligand L on [{ClAuL}2] Systems. *Chem. - Eur. J.* **2011,** *17*, 368-377.
27. Vogt, R. A.; Gray, T. G.; Crespo-Hernández, C. E., Subpico-second Intersystem Crossing in Mono- and Di(organophosphine)-gold(I) Naphthalene Derivatives in Solution. *J. Am. Chem. Soc.* **2012,** *134*, 14808-14817.
28. Zhou, M.; Lei, Z.; Guo, Q. X.; Wang, Q. M.; Xia, A., Solvent Dependent Excited State Behaviors of Luminescent Gold(I) − Silver(I) Cluster with Hypercoordinated Carbon. *J. Phys. Chem. C* **2015,** *119*, 14980-14988.
29. Fu, W. F.; Chan, K. C.; Miskowski, V. M.; Che, C. M., The Intrinsic 3[dσ*pσ] Emission of Binuclear Gold(I) Complexes with Two Bridging Diphosphane Ligands Lies in the Near UV; Emissions in the Visible Region Are Due to Exciplexes. *Angew. Chem., Int. Ed. Engl.* **1999,** *38*, 2783-2785.
30. Yam, V. W. W.; Lo, K. K. W., Luminescent Polynuclear d10 Metal Complexes. *Chem. Soc. Rev.* **1999,** *28*, 323-324.
31. Qian, H.; Zhu, M.; Wu, Z.; Jin, R., Quantum Sized Gold Nanoclusters with Atomic Precision. *Acc. Chem. Res.* **2012,** *45*, 1470-1479.
32. Jia, J. H.; Wang, Q. M., Intensely Luminescent Gold(I) - Silver(I) Cluster with Hypercoordinated Carbon. *J. Am. Chem. Soc.* **2009,** *131*, 16634-16635.
33. Lei, Z.; Wang, Q. M., Homo and Heterometallic Gold(I) Clusters with Hypercoordinated Carbon. *Coord. Chem. Rev., in press* **2017**.
34. Scherbaum, F.; Grohmann, A.; Huber, B.; Krüger, C.; Schmidbaur, H., "Aurophilicity" as a Consequence of Relativistic Effects: The Hexakis(triphenylphosphaneaurio)methane Dication $[(Ph_3PAu)_6C]^{2+}$. *Angew. Chem., Int. Ed. Engl.* **1988,** *27*, 1544-1546.
35. Koshevoy, I. O.; Lin, Y. C.; Karttunen, A. J.; Chou, P. T.; Vainiotalo, P.; Tunik, S. P.; Haukka, M.; Pakkanen, T., Intensely Luminescent Alkynyl - Phosphine Gold(I) - Copper(I) Complexes: Synthesis, Characterization, Photophysical, and Computational Studies. *Inorg. Chem.* **2009,** *48*, 2094-2102.
36. Kordel, M.; Schooss, D.; Neiss, C.; Walter, L.; Kappes, M. M., Laser-Induced Fluorescence of Rhodamine 6G Cations in the Gas Phase: A Lower Bound to the Lifetime of the First Triplet State. *J. Phys. Chem. A* **2010,** *114*, 5509-5514.
37. Greisch, J. F.; Chmela, J.; Harding, M. E.; Klopper, W.; Kappes, M. M.; Schooss, D., Gas-Phase Photoluminescence Characterization of Stoichiometrically Pure Nonanuclear Lanthanoid Hydroxo Complexes Comprising Europium or Gadolinium. *Inorg. Chem.* **2016,** *55*, 3316-3323.
38. Greisch, J. F.; Harding, M. E.; Schäfer, B.; Ruben, M.; Klopper, W.; Kappes, M. M.; Schooss, D., Characterization of Nonanuclear Europium and Gadolinium Complexes by Gas-Phase Luminescence Spectroscopy. *J. Phys. Chem. Lett.* **2014,** *5*, 1727-1731.
39. Kruppa, S. V.; Nosenko, Y.; Winghart, M. O.; Walg, S. P.; Kappes, M. M.; Riehn, C., Fragmentation Pathways of Dianionic $[Pt_2(\mu\text{-}P_2O_5H_2)_4+X,Y]^{2-}$ (X,Y=H,K,Ag) Species in an Ion Trap Induced by Collisions and UV Photoexcitation. *Int. J. Mass spectrom.* **2016,** *395*, 7-19.
40. Kruppa, S. V.; Bäppler, F.; Nosenko, Y.; Walg, S. P.; Diller, R.; Riehn, C., Ultrafast Vibrational and Electronic Dynamics of Metal-Metal Interactions Studied by Transient Photofragmentation (Gas Phase) and Transient Absorption (Solution). *Int. Conf.Ultrafast Phenom.* **2016**, UW4A.33.
41. Nosenko, Y.; Riehn, C.; Klopper, W., UV Fragmentation and Ultrafast Dynamics of Trinuclear Silver/1-methylthymine and Silver/1-methyluracil Metal-base Pairs in an Ion Trap. *Chem. Phys. Lett.* **2016,** *659*, 55-60.
42. Kruppa, S. V.; Bäppler, F.; Klopper, W.; Walg, S. P.; Thiel, W. R.; Diller, R.; Riehn, C., Ultrafast excited-state relaxation of a binuclear Ag(I) phosphine complex in gas phase and solution. *Phys. Chem. Chem. Phys.* **2017,** *19*, 22785-22800.

43. *Frisch, M. J.; Trucks, G. W.; Schlegel, H. B.; Scuseria, G. E.; Robb, M. A.; Cheeseman, J. R.; Scalmani, G.; Barone, V.; Mennucci, B.; Petersson, G. A.; et al. Gaussian 09, Revision D01; Gaussian, Inc.: Wallingford, CT, 2009 (program)*.

44. Yanai, T.; Tew, D.; Handy, N., A New Hybrid Exchange-correlation Functional using the Coulomb-attenuating Method (CAM-B3LYP). *Chem. Phys. Lett.* **2004,** *393*, 51-57.

45. Peach, M. J. G.; Benfield, P.; Helgaker, T.; Tozer, D., Excitation Energies in Density Functional Theory: An Evaluation and a Diagnostic Test. *J. Chem. Phys.* **2008,** *128*, 044118.

46. Hay, P. J.; Wadt, W. R., Ab Initio Effective Core Potentials for Molecular Calculations. Potentials for the Transition Metal Atoms Sc to Hg. *J. Chem. Phys.* **1985,** *82*, 270-283.

47. Hay, P. J.; Wadt, W. R., Ab Initio Effective Core Potentials for Molecular Calculations. Potentials for K to Au Including the Outermost Core Orbitals. *J. Chem. Phys.* **1985,** *82*, 299-310.

48. Foster, J. P.; Weinhold, F., Natural Hybrid Orbitals. *J. Am. Chem. Soc.* **1980,** *102*, 7211-7218.

49. Reed, A. E.; Curtiss, L. A.; Weinhold, F., Intermolecular Interactions from a Natural Bond Orbital, Donor-Acceptor Viewpoint *Chem. Rev.* **1988,** *88*, 899-926.

50. Zavras, A.; Khairallah, G. N.; Connell, T. U.; White, J. M.; Edwards, A. J.; Mulder, R. J.; Donnelly, P. S.; O'Hair, R. A. J., Synthesis, Structural Characterization, and Gas-Phase Unimolecular Reactivity of the Silver Hydride Nanocluster $[Ag_3((PPh_2)_2CH_2)_3(\mu_3\text{-}H)](BF_4)_2$. *Inorg. Chem.* **2014,** *53*, 7429-7437.

51. Lifshitz, C., Kinetic shifts. *Eur. J. Mass Spectrom.* **2002,** *8*, 85-98.

52. Wellman, S. M. J.; Jockusch, R. A., Moving in on the Action: An Experimental Comparison of Fluorescence Excitation and Photodissociation Action Spectroscopy. *J. Phys. Chem. A* **2015,** *119*, 6333-6338.

53. Imanbaew, D.; Nosenko, Y.; Kerner, C.; Chevalier, K.; Rupp, F.; Riehn, C.; Thiel, W. R.; Diller, R.; Bagchi, B., Excited-state Dynamics of a Ruthenium(II) Catalyst Studied by Transient Photofragmentation in Gas Phase and Transient Absorption in Solution. *Chem. Phys.* **2014,** *442*, 53-61.

54. Imanbaew, D.; Lang, J.; Gelin, M. F.; Kaufhold, S.; Pfeffer, M. G.; Rau, S.; Riehn, C., Pump-Probe Fragmentation Action Spectroscopy: A Powerful Tool to Unravel Light-Induced Processes in Molecular Photocatalysts. *Angew. Chem., Int. Ed. Engl.* **2017,** *129*, 5563-5566.

55. Kasha, M.; Rawls, H. R.; El-Bayoumi, M. A., The Exciton Model in Molecular Spectroscopy. *Pure Appl. Chem.* **1965,** *11*, 371-392.

56. Walter, M.; Akola, J.; Lopez-Acevedo, O.; Jadzinsky, P. D.; Calero, G.; Ackerson, C. J.; Whetten, R. L.; Grönbeck, H.; Häkkinen, H., A Unified View of Ligand-protected Gold Clusters as Superatom Complexes. *Proc. Natl. Acad. Sci. U.S.A.* **2008,** *105*, 9157-9162.

57. Hau, F. K. W.; Lee, T. K. M.; Cheng, E. C. C.; Au, V. K. M.; Yam, V. W. W., Luminescence Color Switching of Supramolecular Assemblies of Discrete Molecular Decanuclear Gold(I) Sulfido Complexes. *Proc. Natl. Acad. Sci. U.S.A.* **2014,** *111*, 15900-15905.

58. Yersin, H.; Strasser, J., Chemically Tuned Zero-field Splittings and Spin-lattice Relaxation Investigation by Time-resolved Emission *J. Lumin.* **1997,** *72-74*, 462-463.

59. Chen, P.; Meyer, T. J., Medium Effects on Charge Transfer in Metal Complexes. *Chem. Rev.* **1998,** *98*, 1439-1478.

TOC Graphic